# Long-duration $\gamma$ ray emissions from 2007 and 2008 winter thunderstorms

H. Tsuchiya,[1] T. Enoto,[2] S. Yamada,[3] T. Yuasa,[3] K. Nakazawa,[3] T. Kitaguchi,[4] M. Kawaharada,[5] M. Kokubun,[5] H. Kato,[1] M. Okano,[1] and K. Makishima[3]

Received 7 October 2010; revised 24 January 2011; accepted 23 February 2011; published 14 May 2011.

[1] The Gamma-Ray Observation of Winter Thunderclouds (GROWTH) experiment, consisting of two radiation detection subsystems, has been operating since 2006 on the premises of Kashiwazaki-Kariwa nuclear power plant located at the coastal area of Japan Sea. By February 2010, GROWTH detected seven long-duration $\gamma$ ray emissions associated with winter thunderstorms. Of them, two events, obtained on 13 December 2007 and 25 December 2008, are reported. On both occasions, all inorganic scintillators (NaI, CsI, and BGO) of the two subsystems detected significant $\gamma$ ray signals lasting for >1 min. Neither of these two events were associated with any lightning. In both cases, the $\gamma$ ray energy spectra extend to 10 MeV, suggesting that the detected $\gamma$ rays are produced by relativistic electrons via bremsstrahlung. Assuming that the initial photon spectrum at the source is expressed by a power law function, the observed photons can be interpreted as being radiated from a source located at a distance of 290–560 m for the 2007 event and 110–690 m for the 2008 one, both at the 90% confidence level. Employing these photon spectra, the number of relativistic electrons is estimated as $10^9$–$10^{11}$. The estimation generally agrees with those calculated on the basis of the relativistic runaway electron avalanche model. A GROWTH photon spectrum, summed over three individual events including the present two events and another reported previously, has similar features including a cutoff energy, to an averaged spectrum of terrestrial $\gamma$ ray flashes.

**Citation:** Tsuchiya, H., et al. (2011), Long-duration $\gamma$ ray emissions from 2007 and 2008 winter thunderstorms, *J. Geophys. Res.*, *116*, D09113, doi:10.1029/2010JD015161.

## 1. Introduction

[2] Nonthermal X-ray and $\gamma$ ray emission, typically lasting for a few seconds to ~10 min, has been observed from thunderstorm activity, with detectors on board an airplane [*McCarthy and Parks*, 1985] and a balloon [*Eack et al.*, 1996, 2000], high-mountain detectors [*Suszcynsky et al.*, 1996; *Brunetti et al.*, 2000; *Chubenko et al.*, 2000; *Alexeenko et al.*, 2002; *Muraki et al.*, 2004; *Torii et al.*, 2009; *Tsuchiya et al.*, 2009; *Chilingarian et al.*, 2010], and ground-based ones [*Torii et al.*, 2002; *Tsuchiya et al.*, 2007]. Interestingly, they do not appear to clearly coincide with lightning processes such as stepped leaders or return strokes. In contrast, much shorter energetic radiation bursts, lasting only for tens of milliseconds or less, are often associated with lightning discharges. Though not necessarily homogeneous, they include terrestrial $\gamma$ ray flashes (TGFs) [*Fishman et al.*, 1994; *Smith et al.*, 2005; *Grefenstette et al.*, 2009; *Briggs et al.*, 2010; *Connaughton et al.*, 2010; *Marisaldi et al.*, 2010a, 2010b], natural lightning [*Moore et al.*, 2001; *Dwyer et al.*, 2005; *Howard et al.*, 2008; *Yoshida et al.*, 2008; *Chubenko et al.*, 2009], and rocket-triggered ones [*Dwyer et al.*, 2003, 2004a, 2004b].

[3] In this way, it has recently become clear that apparently two types of radiation bursts with distinct duration are associated with thunderstorm activity. Although it is uncertain whether or not these two types have a common source mechanism, recent observations as well as theoretical works generally suggest that these bursts, especially short-duration ones, are produced by processes involving acceleration and multiplication of a background population of electrons.

[4] Various numerical kinetic calculations [*Gurevich et al.*, 1992; *Roussel-Dupré et al.*, 1994; *Bell et al.*, 1995; *Lehtinen et al.*, 1996; *Gurevich et al.*, 1997; *Milikh and Valdivia*, 1999; *Gurevich et al.*, 2007; *Roussel-Dupré et al.*, 2008] and Monte Carlo simulations [*Lehtinen et al.*, 1999; *Dwyer*, 2003; *Babich et al.*, 2005, 2007] commonly indicate that most of prompt nonthermal photons from lightning discharges are radiated, via bremsstrahlung, by relativistic electrons, which

[1]High-energy Astrophysics Laboratory, RIKEN, Wako, Japan.
[2]Kavli Institute for Particle Astrophysics and Cosmology, Department of Physics and SLAC National Accelerator Laboratory, Stanford University, Stanford, California, USA.
[3]Department of Physics, University of Tokyo, Tokyo, Japan.
[4]Division of Physics, Mathematics, and Astronomy, California Institute of Technology, Pasadena, California, USA.
[5]Department of High Energy Astrophysics, Institute of Space and Astronautical Science, JAXA, Sagamihara, Japan.


0148-0227/11/2010JD015161

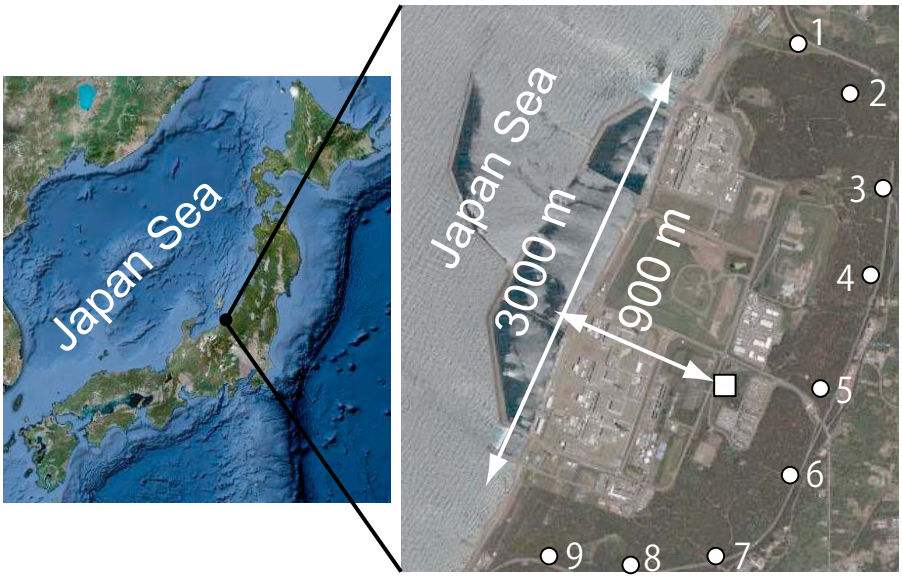


**Figure 1.** (left) The location of the Kashiwazaki-Kariwa nuclear power plant and (right) a bird's eye view. The solid square in Figure 1 (right) represents the GROWTH experimental site, while the nine solid circles show locations of radiation monitors. Each original image is taken from Google Maps.

in turn are produced through mechanism involving relativistic runaway electron avalanche (RREA): some seed electrons, produced by, e.g., cosmic rays, can be accelerated into relativistic regime if they can gain energies from the high electric fields in thunderclouds fast enough to overcome their total energy losses, due mainly to ionization. Then, they collide with air molecules and ionize them. Some of the faster newborn secondary electrons are also accelerated to higher energies, hence increasing in their number. Finally, they will emit a detectable flux of nonthermal photons via bremsstrahlung.

[5] Early observations of long-duration bursts, though limited in number, measured X-ray fluxes in a few keV to a few hundred keV range, or $\gamma$ ray fluxes in MeV regions, suggesting that these prolonged emissions are also due to relativistic electrons [*McCarthy and Parks*, 1985; *Eack et al.*, 1996, 2000; *Brunetti et al.*, 2000; *Chubenko et al.*, 2000]. Several recent observations [*Tsuchiya et al.*, 2007; *Torii et al.*, 2009; *Tsuchiya et al.*, 2009; *Chilingarian et al.*, 2010] have reinforced the suggestion, by detecting photon spectra extending clearly to 10 MeV or higher, and have given evidence that those long-duration $\gamma$ rays are also produced via bremsstrahlung. These results naturally lead to a view that long-duration events are also caused by relativistic runaway electrons. However, compared with short-duration ones, the nature of long-duration bursts have remained less understood, due primary to the lack of a sufficiently large sample. For example, it is still unclear how the electron acceleration process keeps operating for such long durations. In addition, the relation between short-duration bursts and long-duration ones is unknown.

[6] Aiming at detections of radiation bursts from thunderstorm activity, we have been operating the Gamma-Ray Observations of Winter Thunderclouds (GROWTH) experiment since 20 December 2006. In this paper, we report on successful GROWTH detections of two long-duration $\gamma$ ray bursts extending to 10 MeV. Using the acquired $\gamma$ ray data, the source distance, its spatial extent, and the number of relativistic electrons involved therein are estimated. Then, a $\gamma$ ray spectrum which sums up 3 GROWTH detections is compared with cumulative TGF spectra obtained by two independent space observations. Based on these results, we quantitatively discuss the production mechanism of prolonged $\gamma$ ray bursts from winter thunderclouds.

## 2. The GROWTH Experiment

[7] The GROWTH experiment, comprising two independent subsystems, has been operating successfully at a roof of a building of Kashiwazaki-Kariwa nuclear power plant in Niigata Prefecture, Japan. Figure 1 shows the location of the plant, facing the Japan Sea, and the GROWTH experimental site therein. The geographical longitude, latitude, and altitude of the experimental site are 138°36′E, 37°26′N, and 40 m above sea level, respectively. This coastal area is frequently struck by strong thunderstorms in winter seasons. Actually, before the GROWTH experiment started working, radiation monitors (solid circles in Figure 1), which are arranged at around 300–400 m intervals in the plant, occasionally observed >3 MeV intense radiation enhancements in winter seasons, which are difficult to ascribe to so-called radon washouts because these rainfall-related episodes would mainly cause increases at <3 MeV energies [e.g., *Yoshioka*, 1992; *Yamazaki et al.*, 2002]. Each radiation monitor consists of a $\phi$5.1 cm × 5.1 cm NaI (Tl) scintillation counter and a spherical ion chamber with a volume of ~14 L that contains Ar gas. The former covers the 50 keV to 3 MeV energy range, while the latter operates in >50 keV. However, the radiation monitors have too poor a time resolution of 30 s, together with the too limited energy bands, to understand the nature of those phenomena. The GROWTH experiment is

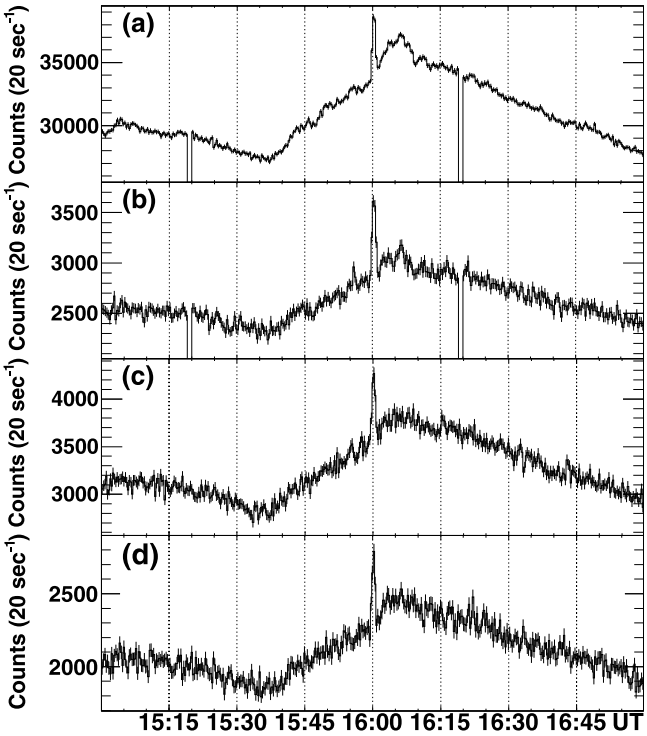


**Figure 2.** Count rates per 20 s of the four inorganic scintillators over 1500–1700 UT on 13 December 2007. (a and b) The >40 keV count rates from the BGO and NaI scintillators without the anticoincidence of detector A, respectively. (c and d) The >40 keV count rates of NaI (>40 keV) and CsI (>300 keV) scintillators of detector B, respectively. Horizontal axis shows universal time. Error bars are statistical $1\sigma$. The gaps in Figures 2a and 2b are due to regular interruptions of data acquisition of detector A every hour.

expected to provide much improved knowledge on these sporadic events.

[8] The pictures and drawings of the two subsystems are given by *Enoto et al.* [2007] and *Tsuchiya et al.* [2007]. One of them (detector A) uses two cylindrical NaI (Tl) scintillators (density is 3.67 g cm$^{-3}$), having a diameter and a height of both 7.62 cm. In order to actively shield them from natural low-energy (<3 MeV) environmental radiation (e.g., from $^{40}$K), the NaI scintillators are individually surrounded by well-shaped BGO ($Bi_4Ge_3O_{12}$; density is 7.1 g cm$^{-3}$) scintillators, with the thickness on the side and bottom being 1.27 and 2.54 cm, respectively. The BGO scintillators geometrically shield the central NaI up to a solid angle of $2.4\pi$ sr, or $0.6 \times 4\pi$. Thus, the NaI scintillators have a higher sensitivity toward the sky direction. The two central NaI scintillators and the BGO shields are operated over an energy range of 40 keV to 10 MeV. Output signals from photomultiplier tubes, attached to NaI and BGO, are fed individually to a 12 bit 8-channel VME analog-to-digital converter (ADC (CP 1113A)) with a time resolution of 10 $\mu$s and are recorded on event-by-event basis.

[9] As another feature of detector A, a 0.5 cm thick plastic scintillator with an area of 30.5 cm × 15.2 cm (= 464 cm$^2$) is placed above the two NaI scintillators and is operated with a threshold energy of >1 MeV. It has a high detection efficiency for charged particles, while it is almost transparent to photons due to its thinness and higher threshold. Utilizing this feature, we can separate charged particles from photons, and efficiently exclude background cosmic ray muons, which typically deposit >1 MeV energies, from events in the two NaI scintillators. Specifically, an event in either of the two NaI scintillators is judged as a charged particle if it give a simultaneous hit (with 10 $\mu$s) in the plastic scintillator. Thus, utilizing signals of the BGO and plastic scintillators both in anticoincidence, the central NaI scintillators effectively detect photons, generally arriving from a sky direction.

[10] Aiming at an independent radiation measurement, another subsystem (detector B) was installed ~10 m apart from detector A. It consists of spherical NaI (Tl) and CsI (Tl) scintillators (density is 4.51 g cm$^{-3}$), both with a diameter of 7.62 cm. The former operates in 40 keV to 10 MeV, while the latter covers a higher energy range of 300 keV to 80 MeV. Unlike detector A, these scintillators have omnidirectional sensitivity because they have no shields such as the BGO or plastic scintillators. Output signals of two photomultiplier tubes, attached to the NaI and CsI crystals, are sampled by a self-triggering electronics system with a 12 bit ADC (AD 574). These events are accumulated into an ADC histogram, which is recorded every 6 s.

[11] Energy calibrations of detectors A and B were carried out, using natural environmental $\gamma$ ray lines of $^{214}$Pb (0.352 MeV), $^{214}$Bi (0.609 MeV), $^{40}$K (1.46 MeV), and $^{208}$Tl (2.61 MeV). Then, especially for the CsI of detector B, cosmic ray muons, giving energy deposits with its peak of around 35 MeV, were also utilized. Basically, these calibrations are performed and checked by an offline analysis.

[12] In addition to those radiation detectors, the GROWTH system utilizes three optical sensors and an electric field mill as environmental monitors. Each optical sensor consists of a hand-made analog circuit, and a silicon photodiode (HAMAMATSU S1226-8BK) which is sensitive over a wavelength range of 320–1000 nm (with its peak at 750 nm). They measure environmental visible light in coarsely different directions; sea side, zenith direction, and antisea side. The output signals are fed to a 12 bit VME-ADC, and recorded every 0.1 s. The electric field mill is a commercial product (BOLTEK EFM-100). Its analog output is fed to a 12 bit ADC (AD 7892), and recored as electric field strength between ±100 kV m$^{-1}$, with a resolution of 50 V m$^{-1}$.

## 3. Results

### 3.1. Count Histories of the Inorganic Scintillators

[13] Figure 2 shows count histories of the four inorganic scintillators of detectors A and B, obtained over 1500–1700 UT on 13 December 2007 which corresponds to local midnight (0000–0200 LT (Japan Standard Time) on 14 December 2007). For reference, typical background rates per 20 s, corresponding to Figures 2a, 2b, 2c, and 2d, are 22000, 1700, 2100, and 1500, respectively. Similarly, Figure 3 gives those over 0830–1030 UT on 25 December 2008 (1730–1930 LT on the same day, or local evening). On both these days, a strong low-pressure system (with ~990 hPa on the ground) developed over Japan, causing thunderstorms at the coastal area of Japan Sea. A gradual count increase, followed by a gradual count decrease, generally shows that

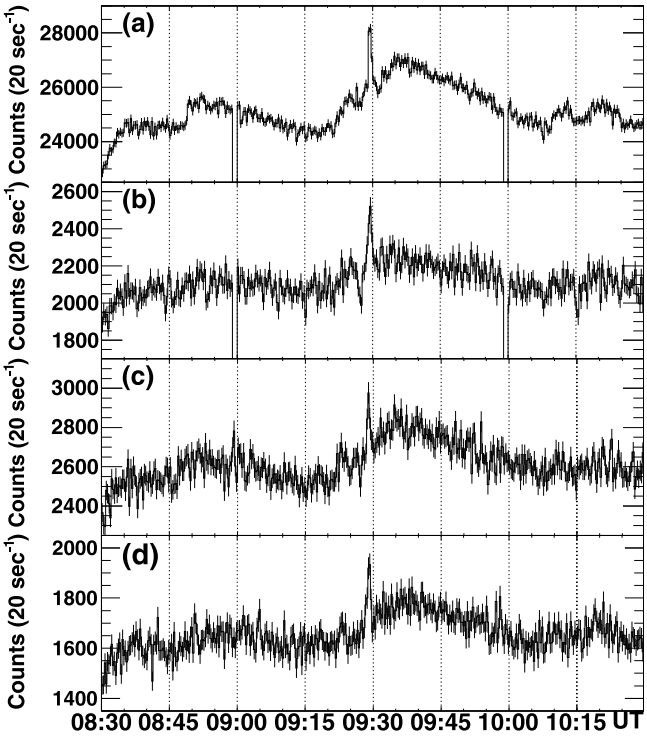


**Figure 3.** Same as Figure 2 but over 0830–1030 UT on 25 December 2008.

they are due mainly to radioactive radon and its decay products in rain, with their half-lives being 20–30 min. These effects originating from radionuclides are closely investigated by *Suszcynsky et al.* [1996] and *Yamazaki et al.* [2002].

[14] Superimposed on such gradual count increases, a sharp count enhancement is found in all the inorganic scintillators at around 1600 UT in Figure 2 and at around 0930 UT in Figure 3. Hereafter, we call the former and the latter events 071213 and 081225, respectively. These enhancements, both lasting for 70–80 s, are quite different from the radon effects and from short radiation bursts associated with lightning discharges. Among those inorganic scintillators, BGO of detector A gave statistically the most significant burst detection on both occasions; $30\sigma$ for 071213 and $19\sigma$ for 081225. This is because it has a higher density and a larger effective atomic number, and hence a higher stopping power, especially for X/$\gamma$ rays, than the other inorganic scintillators used in our system.

[15] Figure 4 shows NaI count histories of 071213 in three energy bands from detectors A and B, and Figure 5 represents those of 081225. For comparison with detector B, the data of detector A (Figures 4a, 4b, 4c, 5a, 5b and 5c) are presented without the BGO or plastic anticoincidence. With a criterion that both the NaI and CsI scintillators of detector B simultaneously record 10 or higher counts per 12 s in the 3–10 MeV energy band, we define burst periods of 071213 and 081225 as 84 s, 1559:29–1600:53 UT, and 72 s, 0928:29–

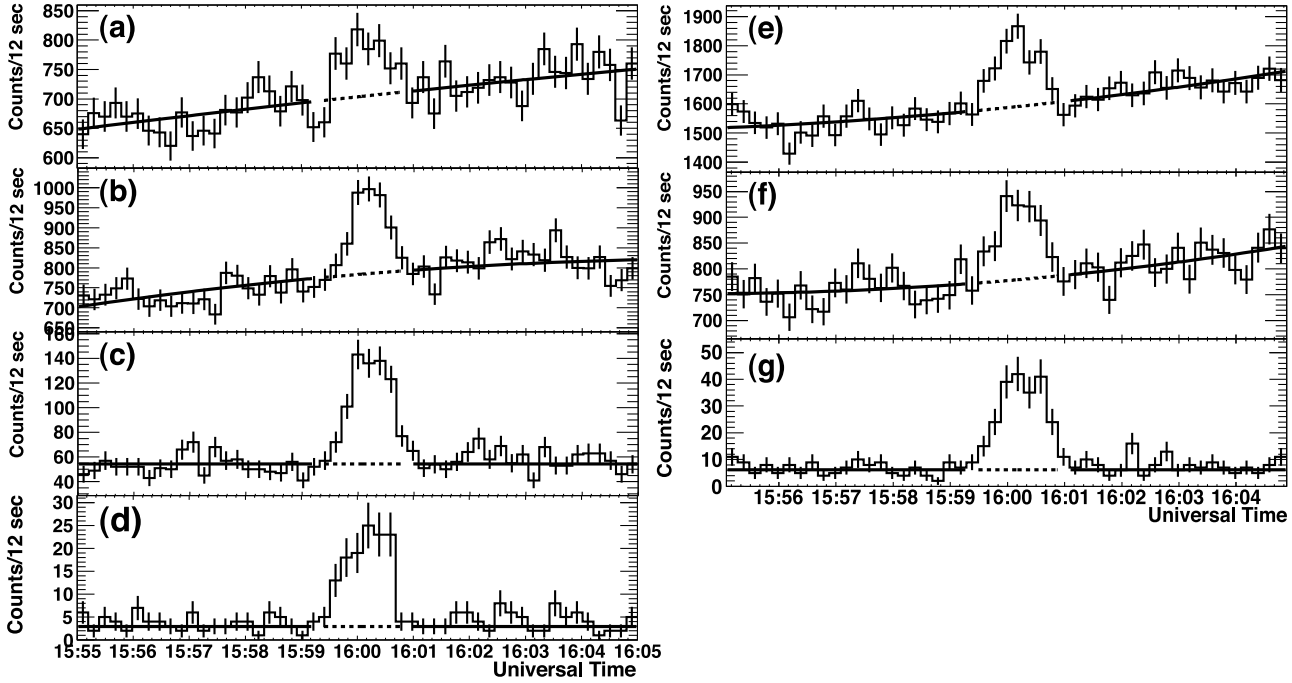


**Figure 4.** Count histories per 12 s of 071213 in three energy bands from (left) detector A (summed over the two NaI) and (right) detector B (NaI), obtained for 1555–1605 UT. (a, b, and c) The 0.04–0.3 MeV, 0.3–3 MeV, and >3 MeV energy bands without anticoincidence, respectively. (d) The >3 MeV energy band of the NaI with anticoincidence. (e, f, and g) Same as Figures 4a, 4b, and 4c, respectively, but for detector B. Solid curves outside the burst period show the estimated background level (see text), while dashed curves denote the interpolated background level over the burst period. Abscissa represents universal time. Each error bar is statistical $1\sigma$.

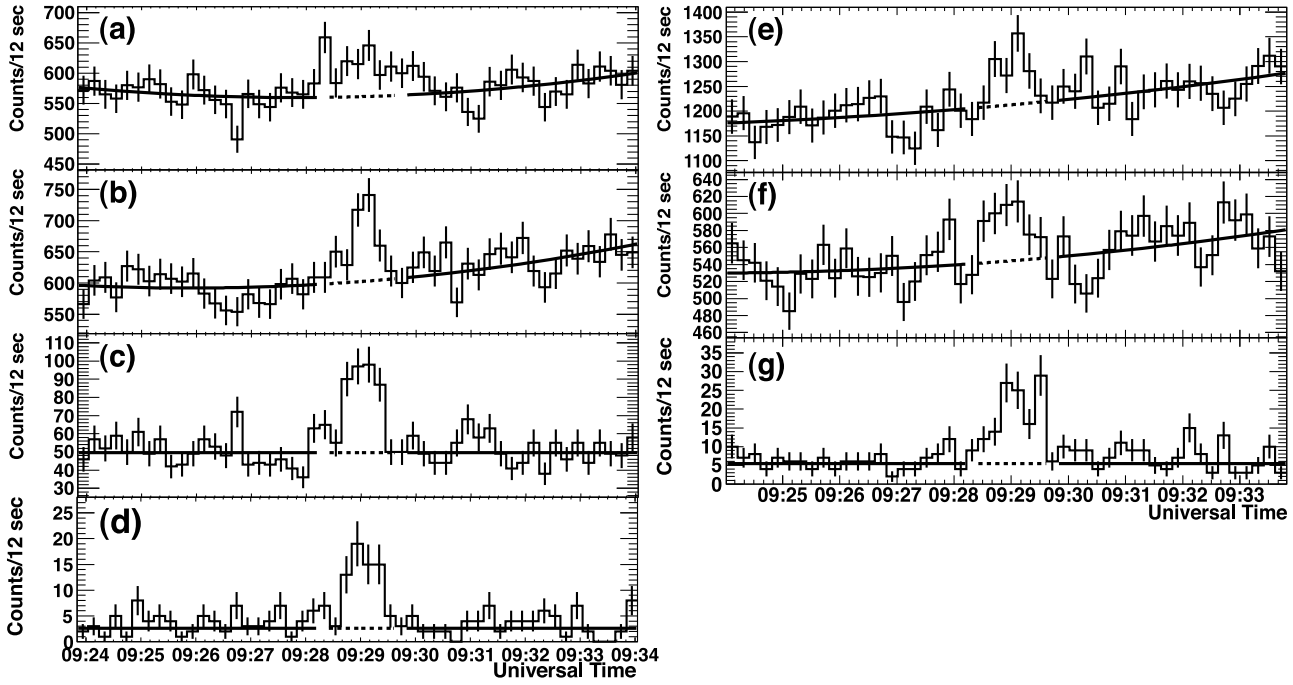


**Figure 5.** Same as Figure 4 but for 081225, obtained over 0924–0934 UT.

0929:37 UT, respectively. For reference, this energy band of either scintillator typically records ~4–5 events per 12 s in quiescent periods; so the above criterion (again, not either but both scintillators have 10 or higher counts) means approximately ≥3.2–4.0 $\sigma$ above the background.

[16] In order to estimate background levels of individual energy bands of detectors A and B, we excluded data over the burst period (as defined above) and the adjacent 12 s periods. The remaining data in the two lower-energy bands were fitted by a quadratic function (via $\chi^2$ evaluation), while those in the highest-energy band with a constant. Table 1 summarizes the net count increases, obtained by subtracting interpolated background (dashed curves of Figures 4 and 5) from the total counts in the burst period. Thus, the burst detection is statistically significant in each of the three energy bands on both occasions. Table 1 also gives the observed photon number fluxes above the detectors using power law spectra obtained later (section 3.5) and the detector responses of detector B derived from a Monte Carlo simulation based on GEANT4 [*Agostinelli et al.*, 2003]. Here, the MC simulation was evaluated with radionuclide sources of $^{60}$Co and $^{137}$Cs.

### 3.2. Arrival Directions

[17] Figures 4 and 5 show the NaI count rates of detector A at >3 MeV energies of 071213 and 081225, respectively, with (Figures 4d and 5d) and without (Figures 4c and 5c) anticoincidence. In Figures 4 and 5, the anticoincidence, which utilizes BGO and plastic signals in logical "OR," is seen to reduce the NaI background level (solid curves) to ~0.05 times that without anticoincidence. In contrast, the NaI-detected burst signal rate decreases due to the anticoincidence only to 0.25 ± 0.03 and 0.31 ± 0.06 times the raw rates for 071213 and 081225, respectively. Thus, the burst photons survive the anticoincidence with 5–6 times higher efficiency than the background events. Similarly, the ratio of the >40 keV NaI (Figures 2b and 3b) to the >40 keV BGO count rates (Figures 2a and 3a), which is normally ~0.08 due mostly to environmental radioactivity coming from omnidirections, increased to 0.18 ± 0.02 for 071213 and 0.14 ± 0.02 for 081225.

[18] The above properties revealed by applying the anticoincidence are thought to reflect arrival directions of the burst signals. If they came mainly from horizontal or ground directions, the anticoincidence on/off ratio and the NaI/BGO

**Table 1.** Count Enhancements and the Corresponding Photon Number Flux of Events 071213 and 081225

| | 071213 | | | 081225 | | |
|---|---|---|---|---|---|---|
| $\Delta E$ (MeV) | Detector A[a] | Detector B[b] | Flux[c] ($\times 10^{-2}$ cm$^{-2}$ s$^{-1}$) | Detector A[a] | Detector B[b] | Flux[c] ($\times 10^{-2}$ cm$^{-2}$ s$^{-1}$) |
| 0.04–0.3 | 530 ± 70 | 1120 ± 110 | 20.2 ± 1.9 | 300 ± 60 | 390 ± 90 | 6.1 ± 1.7 |
| 0.3–3 | 900 ± 80 | 1660 ± 140 | 22.2 ± 2.3 | 400 ± 60 | 920 ± 110 | 7.6 ± 2.1 |
| 3–10 | 410 ± 30 | 370 ± 20 | 10.5 ± 1.0 | 180 ± 20 | 178 ± 16 | 6.8 ± 0.9 |

[a]Sum of the two NaI detectors.
[b]The 0.04–0.3 MeV count correspond to the NaI detector, while the others a sum of the NaI and CsI detectors.
[c]The flux is calculated by the data of detector B.

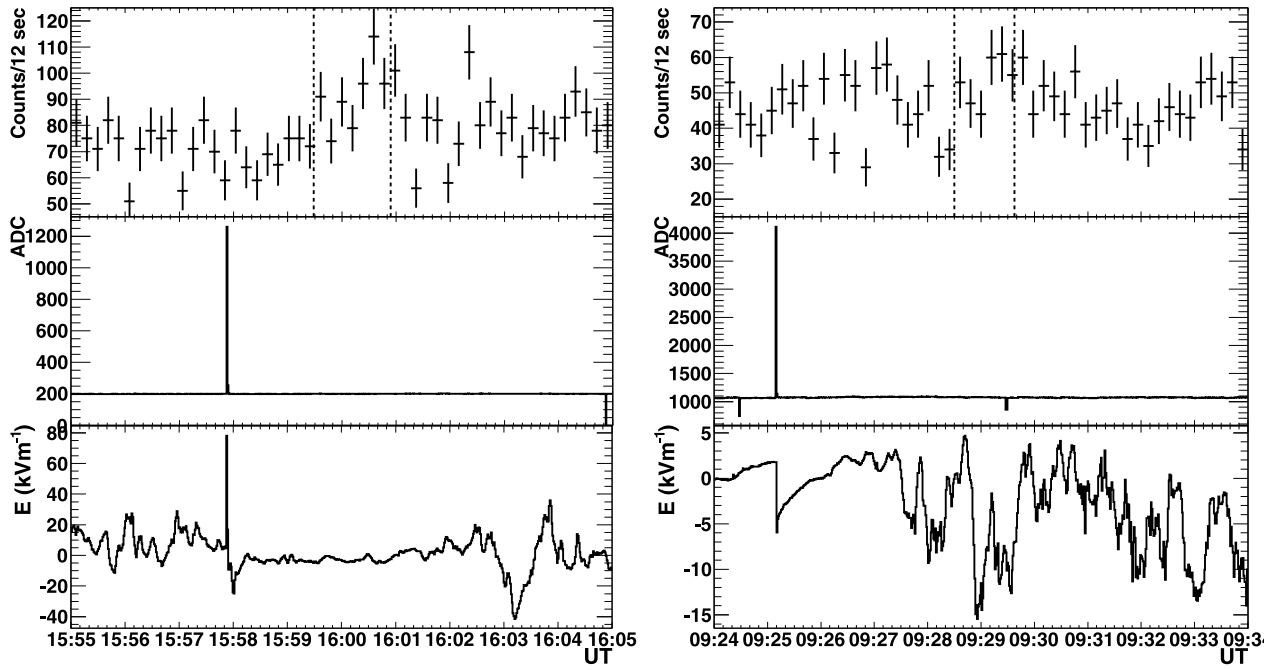


**Figure 6.** The count rate histories of the plastic scintillator of detector A and the environmental sensors. (left) Event 071213, obtained over 1555–1605 UT. (right) Event 081225, obtained for 0924–0934 UT. (top) A >1 MeV counts every 12 s from the plastic scintillator, (middle) 1 s optical data variations, and (bottom) 1 s electric field variations. All abscissa are universal time. Vertical lines in Figure 6 (top) represent the burst periods.

ratio would both fall below their normal values, because, e.g., 40 keV or 3 MeV $\gamma$ rays horizontally entering detector A would be almost fully or partially (at least 30%) absorbed/scattered by BGO via photoelectric absorption and Compton scattering. Accordingly, we conclude that the burst signals arrived from sky directions, not from horizontal or ground directions. A more quantitative study of arrival directions, employing Monte Carlo simulations, will be reported elsewhere.

### 3.3. Burst Components

[19] Figure 6 shows count histories of the plastic scintillator (>1 MeV) and the environmental sensors. In coincidence with the apparent signals detected by the inorganic scintillators, the 0.5 cm thick plastic scintillator gave count increases in individual burst periods by $N_{\rm pl} = 160 \pm 30$ ($5.3\sigma$) for 071213 and $72 \pm 18$ ($4\sigma$) for 081225 (Figure 6, top). Presumably these plastic signals are composed of $\gamma$ rays and charged particles, most likely electrons, which are either accelerated primaries or secondary ones produced by high-energy photons via Compton scattering. Below, we estimate how $\gamma$ rays and electrons contribute to $N_{\rm pl}$, and estimate the electron flux above 1 MeV.

[20] First, a Monte Carlo simulation using GEANT4 predicts that the plastic scintillator has a low detection efficiency, 0.5–1%, for >1 MeV $\gamma$ rays, while that for >1 MeV electrons reaches 75–90%. Next, using power law spectra obtained later (section 3.5) and the effective area of the NaI scintillator of detector B yield 1–10 MeV photon number fluxes above the GROWTH system as $(17.9 \pm 1.8) \times 10^{-2}$ cm$^{-2}$ s$^{-1}$ for 071213, and $(9.2 \pm 1.8) \times 10^{-2}$ cm$^{-2}$ s$^{-1}$ for 081213. Then, multiplying these fluxes by the GEANT4-derived detection efficiency for $\gamma$ rays of the plastic scintillator and the area of the plastic scintillator, 464 cm$^2$, $\gamma$ ray produced counts contributing to $N_{\rm pl}$ are estimated as $N_\gamma = 70 \pm 7$ for 071213, and $31 \pm 6$ for 081225. Finally, subtracting $N_\gamma$ from $N_{\rm pl}$, the contribution of electrons is obtained as $90 \pm 30$ for 071213, and $41 \pm 19$ for 081225. Although these numbers, when taken at their face values, imply a significant electron contribution to $N_{\rm pl}$, here we conservatively regard them as upper limits. Then, a 95% confidence level upper limit on the electron flux above 1 MeV of 071213 and 081225 is computed as $0.5 \times 10^{-2}$ cm$^{-2}$ s$^{-1}$ and $0.3 \times 10^{-2}$ cm$^{-2}$ s$^{-1}$, respectively. These upper limits are more than an order of magnitude lower than the 1–10 MeV $\gamma$ ray fluxes. Therefore, the observed burst signals arriving at the GROWTH system are inferred to be dominated by photons, rather than electrons.

### 3.4. Comparison With Signals From Environmental Sensors

[21] The visible light sensor (Figure 6, middle) recorded an extremely intense signal, lasting ≤1 s, at 1557:50 UT and 0925:09 UT for 071213 and 081225, respectively. In coincidence with the recorded optical flashes, the electric field rapidly changed its polarity from positive to negative (Figure 6, bottom). These indicate that a lightning discharge occurred. However, their occurrence is well separated from the $\gamma$ ray bursts themselves, namely, 100 and 180 s prior to the 071213 and 082125 commencements, respectively. Thus, we con-

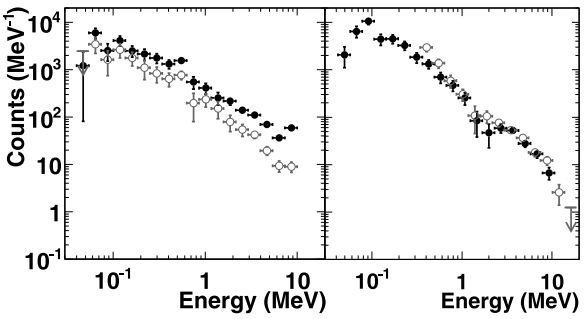


**Figure 7.** Background-subtracted spectra of detectors (left) A and (right) B of 071213. Black and gray points in Figure 7 (left) indicate the NaI data without and with anticoincidence, respectively, while those in Figure 7 (right) show the NaI and CsI scintillators, respectively. All error bars quoted are statistical $1\sigma$. Arrows, showing 95% confidence level upper limits, are drawn when statistical significance of a data point is lower than $1\sigma$. The horizontal and vertical axes show the photon energy in MeV and count per unit energy interval, respectively. Detector responses have not been removed.

clude that neither of the present two $\gamma$ ray bursts coincided with lightning discharges.

[22] Prior to the present work, *Tsuchiya et al.* [2007, 2009] have reported similar lack of coincidence between prolonged $\gamma$ ray bursts and lightning discharges. *Tsuchiya et al.* [2007] detected a long-duration burst, lasting 40 s, using the GROWTH system 70 s prior to lightning, while *Tsuchiya et al.* [2009] measured no lightning discharges over 5 min before or after a prolonged (~90 s) burst was detected at a high-mountain detector. These previously reported events, observed during thunderstorms, have also been considered to be associated with thunderclouds.

[23] In the same manner, we associate the present bursts with the thunderclouds, rather than with lightning discharges. Actually, rainfall-thunder observation data (rainfall-thunder observation data are available from http://thunder.tepco.co.jp/), provided by a laser observation system operated by Tokyo Electric Power Company, showed that thunderclouds approached the Kashiwazaki-Kariwa nuclear plant from the sea side on both occasions and passed over it during the 10 min.

### 3.5. Energy Spectra

[24] Figures 7 and 8 show background-subtracted GROWTH spectra, obtained in the burst periods of 071213 and 081225, respectively. In either case, we accumulated the data over the burst period and subtracted background spectra which were averaged over 10 min before and after the burst, although thunderstorms were ongoing during these time periods. This is to remove <3 MeV line $\gamma$ rays induced mainly by radon decays, which increase the background level by up to twice. To examine how the background selection affects the final spectra (Figures 7 and 8), we subtracted an alternative background spectrum averaged over 5 min before and after the burst. However, the background-subtracted spectra did not change by more than ±10% at <1 MeV, or ±5% at >1 MeV. These are almost negligible compared with the statistical errors.

[25] In both events, the background-subtracted spectra of detectors A and B exhibit very hard continuum spectra, which clearly extend to 10 MeV. As shown in another GROWTH event 070106 reported previously [*Tsuchiya et al.*, 2007], and in high-mountain observations [*Torii et al.*, 2009; *Tsuchiya et al.*, 2009; *Chilingarian et al.*, 2010], similar prolonged $\gamma$ ray emissions, extending to 10 MeV or higher, were observed, and have been thought to be produced via bremsstrahlung. Thus, the present high-energy $\gamma$ rays must also be produced via bremsstrahlung by electrons accelerated beyond 10 MeV. Given these results, the present two events, together with the previous ones, may be understood as manifestations of a common type of high-energy activity in thunderstorms.

[26] As easily seen in Figures 7 and 8, the obtained spectra, in particular, those of detector B, flatten in 0.8–3 MeV, even though they are not corrected for the detector responses. One of the causes of this flat is the Compton scattering: since the Compton scattering cross section in the atmosphere increases as photon energy decreases toward 0.1 MeV, photons at low energies would experience stronger Compton degradation than higher-energy ones.

### 3.6. Model Fits

[27] Supposing that the burst $\gamma$ rays were produced in a source located at a certain distance and propagated through atmosphere to reach our detectors, we may deduce the initial photon spectrum at the source, and estimate the source distance, from the background-subtracted spectra. Since the detector A spectra are complicated due to the passive and active shielding effects by the BGO well, below we analyze the detector B spectra. According to numerical calculations [*Roussel-Dupré et al.*, 1994; *Roussel-Dupré and Gurevich*, 1996; *Lehtinen et al.*, 1999; *Babich et al.*, 2007], an energy distribution function of runaway electrons, generated under the RREA mechanism, is expressed by a power law function, or more precisely, an exponentially cutoff power law. Consequently, we assume an initial photon number spectrum as

$$f(\epsilon_p) = \alpha \epsilon_p^{-\beta} \exp(-\epsilon_p/\epsilon_c) \ (\mathrm{MeV^{-1}\,sr^{-1}}). \quad (1)$$

Here, $\alpha$ and $\beta$ are a normalization factor and a photon index, respectively, while $\epsilon_p$ and $\epsilon_c$ describe the emitted photon energy and a cutoff energy in MeV, respectively. While this equation represents an exponentially cutoff power law, it can also express a pure power law by requiring $\epsilon_c \to \infty$.

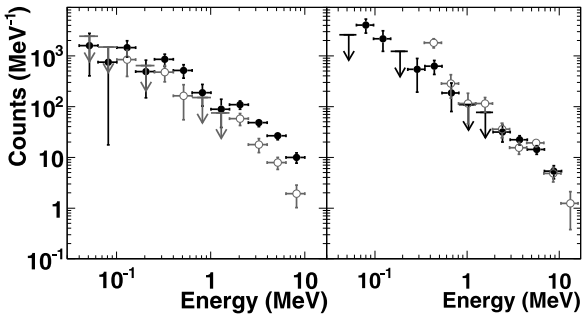


**Figure 8.** Same as Figure 7 but for the 081225 event.

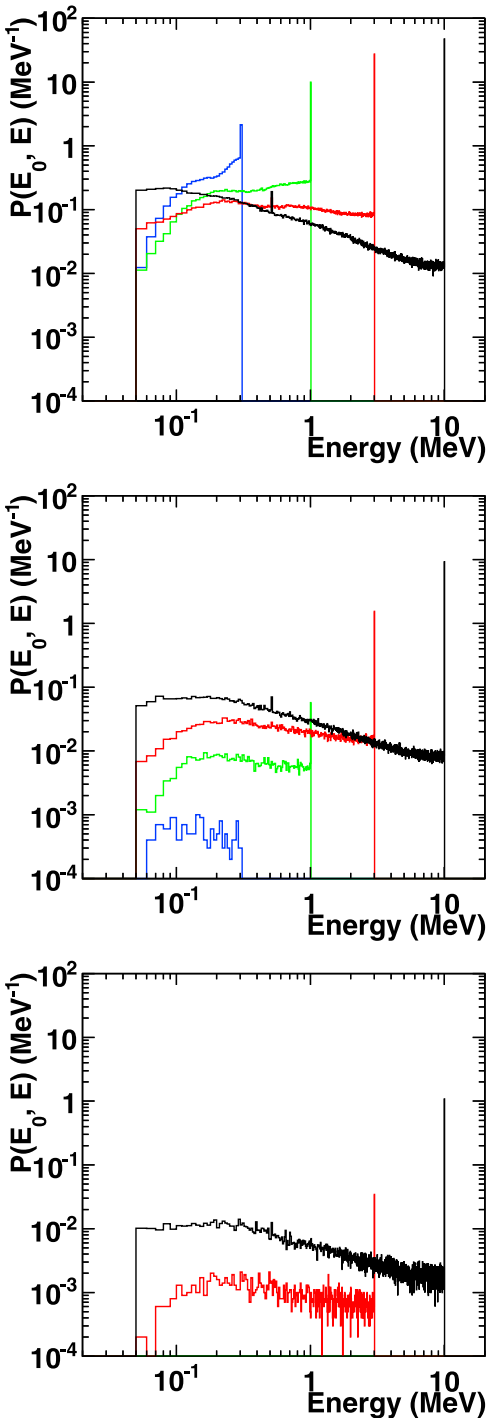


**Figure 9.** Photon spectra at the observatory derived from Monte Carlo simulations for $d$ of (top) 300 m, (middle) 1000 m, and (bottom) 2000 m. Different colors denote incident photon energies, $E_0 = 0.3$ (blue), 1 (green), 3 (red), and 10 MeV (black). Abscissa shows the photon energy at the observatory, while ordinate represents probability density function.

[28] Below, let us estimate the source distance $d$ from our detector B data, as well as $\alpha$, $\beta$, and $\epsilon_c$. In order to simulate the photon propagation in the atmosphere, we utilize EGS4 [*Nelson et al.*, 1985] embedded in CORSIKA 6.500 [*Heck et al.*, 1998]. In the CORSIKA simulation, the atmosphere consists of $N_2$, $O_2$, and Ar with the mole ratios of 78.1%, 21.0%, and 0.9%, respectively. The density of the atmosphere, divided into 5 layers, depends exponentially on the altitude $h$, with a form of $A + B \exp(-h/C)$, with $A$, $B$, $C$ being model parameters. For example, at $h < 4$ km, the model is specified as $A = -186.6$ g cm$^{-2}$, $B = 1222.7$ g cm$^{-2}$, and $C = 9.94$ km [*Heck and Pierog*, 2009]. In addition, EGS4 can adequately treat electromagnetic processes in the relevant energy range of a few tens of keV to a few tens of MeV.

[29] Monoenergetic photon simulations were carried out for 33 incident energies from 50 keV to 100 MeV. The energy interval is set to 10 keV for 50–90 keV, 100 keV for 100 keV to 1 MeV, 1 MeV for 1–10 MeV, and 10 MeV for 10–100 MeV. For one monoenergetic photon simulation, one million photons were vertically injected to the atmosphere from a fixed source distance. In reality, 20 source distances from 20 m to 2000 m were applied for one monoenergetic simulation. Then, we saved the energy, angle, and species of all of photons and particles that arrive at the observatory level (40 m above sea level).

[30] Figure 9 indicates three representative sets of simulated photon spectra, propagating over $d = 300$ m (36 g cm$^{-2}$), 1000 m (120 g cm$^{-2}$), and 2000 m (220 g cm$^{-2}$), with the numbers in parentheses giving air mass calculated by the above exponential formula. Punch-through photons, which suffer no interactions with air molecules, appear as a strong peak at the highest end of each photon spectrum, while scattered ones form a continuum toward lower energies. As the distance increases, the punch-through photons and the scattered continuum are both strongly attenuated, in particular toward lower energies, due primarily to Compton scattering. For instance, the survival probability for 10 (1) MeV punch-through photons to propagate over $d = 2000$ m is only 0.02 ($10^{-5}$) times that over $d = 300$ m. Note that as discussed in section 4.3, a long-duration burst probably changes in the burst period its viewing angle relative to a beam axis of electrons accelerated in thunderclouds. Thus, the calculated photon spectra here would vary according to the changes, and hence they will be treated in this work as ones averaged over different viewing angles.

[31] Convolving the simulated photon spectra with the detector responses, we can obtain a model-predicted spectrum to be observed by the NaI and CsI scintillators. Finally, we convolve these model predictions with the assumed source photon spectrum, equation (1) and fit the predictions simultaneously to the background-subtracted NaI and CsI spectra (Figures 7, right, and 8, right). Then, the model parameters, such as $\alpha$, $\beta$ and $\epsilon_c$, can be determined so as to minimize the fit $\chi^2$.

[32] Figure 10 shows three representative model fits to the spectra of 071213 and 081225, assuming a power law model. The choice of $d$ of 300, 1000, and 2000 m in Figure 10, respectively, gave $\chi^2$ values as 48.4, 77.5, and 116 for 071213 and 40.9, 46.7, and 51.4 for 081225. By changing $d$ and repeating the fitting, we obtained $\chi^2$ curves as shown in Figure 11, together with the $\chi^2$ minima as 46.5 at $d = 400$ m for 071213 and 40.9 at $d = 300$ m for 081225. From Figures 10 and 11, we can constrain source distance. Tables 2 and 3 summarize the best fit parameters for 071213 and 081225, respectively, together with the constrained source distance. Also, low-energy parts (<300 keV) of the two spectra

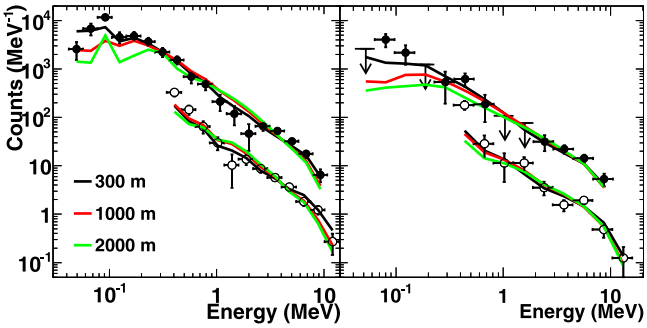


**Figure 10.** The photon spectra observed by the NaI (solid circles) and CsI (open circles) scintillators of detector B, compared with calculations for assumed source distances of 300 m (black), 1000 m (red), and 2000 m (green) for events (left) 071213 and (right) 081225. For clarity, the CsI data and the corresponding model spectra are multiplied by 0.1. The horizontal and vertical axes show the photon energy in MeV and counts in each bin, respectively.

are found to play an important role to determine $d$. If we use the background averaged over the 5 min intervals (instead of 10 min), the source distances become 350 m for 071213 and 300 m for 081225. Thus, the distance is not affected significantly by the systematic background uncertainty.

[33] The NaI and CsI spectra have been explained, in either event, by a common set of model parameters, although the fits are not necessarily good enough. The cutoff energy $E_c$ was constrained to be rather high with relatively large errors. Thus, our data do not provide evidence for spectral cutoff in either event. In agreement with this, the two spectral models, a power law and an exponentially cutoff power law, gave similar goodness of fits in both events. Importantly, the source distance have been constrained with a reasonable accuracy.

[34] As another attempt, we tentatively fixed $E_c$ at 7 MeV, which is the expected average kinetic energy of runaway electrons (not of bremsstrahlung photons), and repeated the model fitting. Then, the fit became worse in both events (Exp PL in Tables 2 and 3). Therefore, the initial photon spectrum is again inferred to extend beyond ~7 MeV.

## 4. Discussion

### 4.1. Source Heights

[35] Assuming a power law function at the source, the $\gamma$ ray spectra of 071213 and 081225 suggest that the sources are located at 290–560 m (35–67 g cm$^{-2}$) and 120–690 m (14–82 g cm$^{-2}$) above our system, respectively, both at 90% confidence level. In fact, these constraints are in good agreement with the known heights of winter thunderclouds in this area. Winter thunderclouds and winter lighting observed at the coastal area of the Japan Sea exhibit many features that have infrequently been found compared to those in summer seasons and/or in other areas [e.g., *Rakov and Uman*, 2005, and references therein]. These include rather low altitudes of the development of these thunderclouds. Actually, *Goto and Narita* [1992] conducted video observations of winter lightning at the same Niigata Prefecture as our experimental site and reported that the visible bases of winter thunderclouds are typically located at 200–800 m above sea level. Also, a recent numerical calculation done by *Babich et al.* [2010] shows that another GROWTH event [*Tsuchiya et al.*, 2007] may be produced at a source height of 0.5–2 km and, hence, generally agrees with the present results.

[36] These height estimations provide an additional clue to the possible electron contributions to the detected plastic signals (section 3.3). As argued so far, electrons are considered to be accelerated in these thunderclouds to at least 10 MeV, probably a few tens of MeV. Since such electrons have a range of <100 m at near the sea level, they would hardly reach our system, even if a range straggling is taken into account. Therefore, it is reasonable that the electron flux incident on our system, if any, was much lower than that of photons.

[37] Unlike the present sea level observations, some high-mountain experiments, conducted at Mount Norikura (2770 m) in Japan [*Tsuchiya et al.*, 2009] and Mount Aragatz (3250 m)

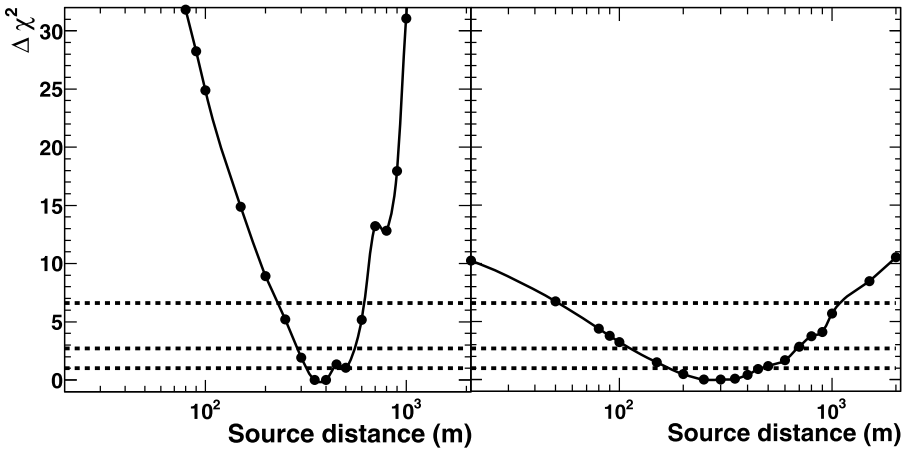


**Figure 11.** The values of $\Delta\chi^2 = \chi^2 - \chi^2_{min}$, plotted as a function of the assumed source distances (black circles) for events (left) 071213 and (right) 081225. Black curves are smoothing lines. Horizontal dashed lines from bottom to top correspond to 68%, 90%, and 99% confidence level.

**Table 2.** Obtained Spectral Parameters and $\chi^2$/d.f. of Event 071213

| | PL[a] | Exp PL[b] | Exp PL (Fix)[c] |
|---|---|---|---|
| $\alpha$ (MeV$^{-1}$ sr$^{-1}$) | $(1.25 \pm 0.03) \times 10^{11}$ | $(7.19 \pm 0.02) \times 10^{10}$ | $(4.9 \pm 0.6) \times 10^{9}$ |
| $\beta$ | $2.03 \pm 0.02$ | $1.88 \pm 0.01$ | $1.2 \pm 0.1$ |
| $\epsilon_c$ (MeV) | – | $50 \pm 20$ | 7 |
| $\chi^2_{min}$/d.f.[d] | 46.5/28 (1.6%) | 46.0/27 (1.3%) | 49.6/28 (0.72%) |
| $d$[e] (m) | $400^{+160}_{-110}$ | $350^{+210}_{-240}$ | $150^{+60}_{-70}$ |

[a]Power law model.
[b]Exponentially cutoff power law model.
[c]Exponentially cutoff power law with $\epsilon_c$ being fixed at 7 MeV.
[d]Values in parentheses represent the probability with the given $\chi^2_{min}$ and degrees of freedom (d.f.).
[e]Quoted errors of $d$ are 90% confidence values, while other errors are 68% ones.

in Armenia [*Chilingarian et al.*, 2010], have detected primary electrons in long-duration events (numbers in parentheses indicate altitudes of observatories). *Tsuchiya et al.* [2009] estimated the source height as 60–130 m (90% confidence level), while *Chilingarian et al.* [2010] evaluated it as 100–150 m. These low source heights, which are comparable to or shorter than the expected electron range, can naturally explain their electron detections.

### 4.2. Extent and Motion of the $\gamma$ Ray Beams

[38] Measuring electric field structure of winter thunderclouds, *Kitagawa and Michimoto* [1994] revealed that tripole electrical structures, which consist of positive, negative and positive layers from top to bottom, appear at mature stages of winter thunderclouds. Then, they observed the tripole structures to last for <10 min in early or late winter, while less than several minutes in midwinter. Since the present two events were observed in midwinter, the measured burst periods of 84 s of 071213 and 72 s of 081225 are consistent with their observations, if the burst durations represent the lifetime of electric fields.

[39] Figure 12 shows dose variations on 13 December 2007, measured by the nearest and the second nearest radiation monitors of the power plant (5 and 6 in Figure 1, black and red lines in Figure 12, respectively). The two monitors gave moderate dose increases for ~1 min or less around the GROWTH event. By examining the GROWTH data of 071213 burst (crosses in Figure 12), as well as dose rates of the second nearest monitor (red line) obtained for 1559:30–1601:00 UT and that of the nearest one (black line) obtained over 1600:00–1601:30 UT, peak times of their enhancement can be evaluated as 1559:48 UT (±6 s), 1559:58 UT (±15 s), and 1600:27 UT (±15 s). Thus, referring to the GROWTH data, the second nearest monitor increased in its dose rates with a small delay of $10 \pm 16$ s (or almost simultaneously), while the nearest one with a larger delay by $39 \pm 16$ s. The two monitors are located at a distance of 500–600 m from the GROWTH system. For reference, data of the other two radiation monitors (4 and 7 in Figure 1) exhibited no apparent increases (green and blue lines in Figure 12). As for 081225, data of those radiation monitors were unavailable due to some data storage problem.

[40] These simultaneous and delayed detections by the two radiation monitors have two important implications. One is that the $\gamma$ ray emission from thunderclouds is likely to have illuminated a rather limited area, spreading over ~600 m on the ground. This kind of effect was also suggested by five radiation monitors (1–5 in Figure 1), on the occasion of the other GROWTH event [*Tsuchiya et al.*, 2007], and another experiment conducted on the same coastal area [*Torii et al.*, 2002]. The other is that the $\gamma$ ray emitting region moved, presumably together with the thunderclouds.

[41] From data of Japan Meteorological Agency, it is found that southwest wind was blowing during 10 min including the burst period of 071213. Thus, the southwest direction can naturally explain the delay of the nearest monitor, if the $\gamma$ ray emitting region moved together with the thunderclouds. Then, the wind velocity was on average 360 m min$^{-1}$, with the maximum of 720 m min$^{-1}$. Projecting, to southwest axis, the distance between the GROWTH system and the nearest monitor, ~500 m, and dividing the projected distance, ~350 m, by its delay, $39 \pm 16$ s, we obtain an average moving velocity of the emitting region as $540 \pm 220$ m min$^{-1}$. Thus, the estimated moving velocity is generally consistent with the wind velocity.

[42] Given above discussions, we may assume that the winter thunderclouds moved from the Japan sea in southwest side to the inland in northeast side. Then, a short-lived tripole structure appeared in a thundercloud and accelerated ambient fast electrons toward the bottom positive layer. The accelerated electrons emitted $\gamma$ rays toward the ground, which the GROWTH system and the two radiation monitors detected when the beam passed over them. The differences in the statistical significance of detections between the GROWTH system and the radiation monitors may be due to different positions and effective viewing angles relative to the accelerated electron beam axis in the thundercloud, and to the differences in their sensitivity. The 081225 event is considered to have occurred under similar conditions, because west winds, with almost the same velocity as in the 071213 case, were blowing at that time. However, it is presently unclear whether the $\gamma$ ray emission ceased when the tripole structure disappeared, or when the $\gamma$ ray beam

**Table 3.** Obtained Spectral Parameters and $\chi^2$/d.f. of Event 081225

| | PL | Exp PL | Exp PL (Fix) |
|---|---|---|---|
| $\alpha$ (MeV$^{-1}$ sr$^{-1}$) | $(1.21 \pm 0.09) \times 10^{9}$ | $(6.4 \pm 1.0) \times 10^{9}$ | $(5.1 \pm 0.4) \times 10^{8}$ |
| $\beta$ | $1.61 \pm 0.03$ | $1.48 \pm 0.09$ | $0.87 \pm 0.02$ |
| $\epsilon_c$ (MeV) | – | $70 \pm 80$ | 7 |
| $\chi^2_{min}$/d.f. | 40.9/20 (0.38%) | 40.6/19 (0.25%) | 43.8/20 (0.16%) |
| $d$ (m) | $300^{+390}_{-180}$ | $250^{+430}_{-210}$ | $100^{+280a}$ |

[a]The lower value was unable to be determined.

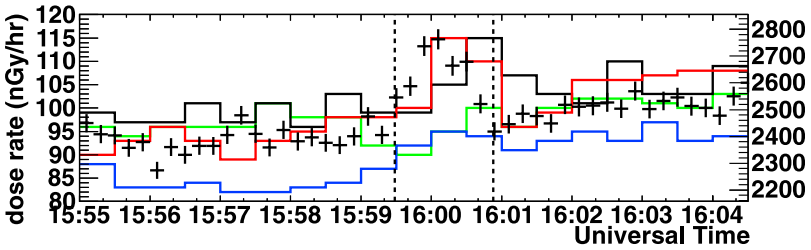


**Figure 12.** Radiation dose rates per 30 s (left ordinate) obtained by ion chambers of radiation monitors over 1555–1605 UT on 13 December 2007. Different colors specify the radiation monitors numbered as 4 (green), 5 (black), 6 (red), and 7 (blue) in Figure 1. Superposed are crosses showing the >40 keV count history per 12 s of the NaI detector of detector B (right ordinate).Vertical dashed lines represent the defined start and end time of the 071213 event.

moved away from the GROWTH system as the thunderclouds moved.

### 4.3. The Number of Relativistic Electrons in Thunderclouds

[43] Using the initial photon energy spectrum $f(\epsilon_p)$ of equation (1) as quantified in Tables 2 and 3, we can estimate the number of relativistic electrons radiating the observed 1–10 MeV $\gamma$ rays via bremsstrahlung, as

$$N_e \sim \frac{2\pi}{H}\int_1^{10} dK_e \int_1^{K_e} d\epsilon_p \int_0^{\theta_{max}} \frac{f(\epsilon_p)}{\eta(K_e,\epsilon_p,\theta)}\sin\theta d\theta. \quad (2)$$

Here, $\eta(K_e, \epsilon_p, \theta)$ is the probability per 1 g cm$^{-2}$ with which an electron with a kinetic energy $K_e$ emits a bremsstrahlung photon with an energy $\epsilon_p$ at an angle $\theta$ with respect to the electron beam axis [*Koch and Motz*, 1959], and $H$ denotes the vertical length of the acceleration region. Since this $H$ is unavailable from the present observations like those of *Tsuchiya et al.* [2009], we assume either $H$ = 300 or 1000 m, corresponding to 35 and 110 g cm$^{-2}$, respectively. These assumptions are based on intracloud observations of X rays using a balloon-borne detector, which showed that a high electric field region, to produce a significant flux in 3–120 keV energy range, has a vertical extent of ~500 m, at altitudes of 3.7–4.2 km [*Eack et al.*, 1996].

[44] We further assumed that the electric-filed strength in the acceleration region is 300 kV m$^{-1}$, which is slightly higher than the threshold (at 1 atm) to cause the runaway electron avalanches. When 1 MeV electrons are accelerated from the top of this acceleration region to the bottom, they will gain energies of 15 MeV for $H$ = 300 m, and 19 MeV for $H$ = 1000 m. Therefore, the assumed electric field strength, together with the assumed vertical length, is sufficient to produce 10 MeV photons via bremsstrahlung.

[45] To calculate, e.g., equation (2), we further need to specify $\theta$; this is suggested to be relatively small, from the obtained photon spectra. In practice, the angle of prolonged $\gamma$ ray event may vary according to the motion of thunderclouds. Thus, we adopt 15° or 30° as $\theta_{max}$. As listed in Table 4, these assumptions, together with equation (1), give $N_e$ = $10^9$–$10^{11}$. Similar estimations for other long-duration $\gamma$ ray bursts have given $N_e$ = $10^8$–$10^{12}$ [*Tsuchiya et al.*, 2007, 2009; *Chilingarian et al.*, 2010]. Thus, long-duration $\gamma$ ray bursts appear to be emitted by a similar number of relativistic electrons.

### 4.4. Relation Between the Bursts and the RREA Mechanism

[46] A possible source of energetic seed electrons to cause the RREA can be attributable to secondary cosmic rays [*Gurevich et al.*, 1992]. The cosmic ray flux above 1 MeV, at the presently relevant altitudes of <1 km, is $I_0 \sim 200$ m$^{-2}$ s$^{-1}$ [*Grieder*, 2001]. Considering the measured burst periods of 70–80 s and the 30–40 s delay of one radiation monitor from the 071213 event, we presume that the acceleration region has a horizontal length of $L \sim 600$ m at most, as judged from the extent of the $\gamma$ ray beam of 071213. Possibly, an actual extent of the acceleration region in thunderclouds would be shorter than this 600 m, because the $\gamma$ ray beam would diverge due to multiple scatterings of the emitting electrons and Compton scatterings of the emitted $\gamma$ rays. We may also consider that an acceleration region is sustained in thunderclouds at least for 100 s. Accordingly, the number of cosmic rays $S_0$, entering the acceleration region, is described as

$$S_0 = 7.2\times10^9 \times (L/600\text{ m})^2 \times \Delta t/100\text{ s}. \quad (3)$$

[47] Based on the RREA mechanism, the total number of relativistic electrons at the end of an acceleration region, $N_{RREA}$, is estimated as

$$N_{RREA} = S_0\exp(\delta),\ \delta = \int_0^H \frac{dz}{\lambda}. \quad (4)$$

The length parameter $\lambda$ is given as

$$\lambda = \frac{7300\text{ kV}}{E - (276\text{ kV m}^{-1})n}\text{ m}, \quad (5)$$

where $E$ is the electric field strength in kV m$^{-1}$ and $n$ denotes the air density relative to that at 1 atm. Equation (5) is valid for 300–3000 kV m$^{-1}$ [*Dwyer*, 2003]. Assuming

**Table 4.** $N_e$ Estimated for Events 071213 and 081225

| | 071213 | | 081225 | |
|---|---|---|---|---|
| $\theta_{max}$ (deg) | $H$ = 300 m | $H$ = 1000 m | $H$ = 300 m | $H$ = 1000 m |
| 15 | $1.9\times10^{10}$ | $6.2\times10^9$ | $3.7\times10^9$ | $1.2\times10^9$ |
| 30 | $4.7\times10^{11}$ | $1.5\times10^{11}$ | $9.3\times10^{10}$ | $3.0\times10^{10}$ |

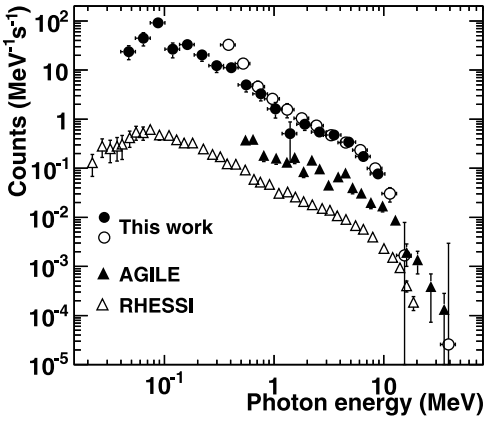


**Figure 13.** Cumulative spectra of the three GROWTH events from detector B (NaI and CsI (solid and open circles, respectively)), compared with summed TGF spectra by RHESSI and AGILE. The latter two spectra are adopted from Figure 2 of *Dwyer and Smith* [2005] and Figure 5 of *Marisaldi et al.* [2010a]. For clarity, the RHESSI and AGILE spectra are multiplied by $1 \times 10^{-5}$ and $1 \times 10^{-4}$, respectively. The vertical and horizontal axes represent counts in MeV$^{-1}$ s$^{-1}$ and photon energy in MeV, respectively. Errors assigned to the GROWTH and AGILE data are statistical ones, while those for RHESSI include systematic uncertainty of background estimation [*Dwyer and Smith*, 2005].

$E = 300$ kV m$^{-1}$ gives $\lambda \sim 300$ m at $P = 1$ atm. In practice, $E$ may be somewhat lower than 300 kV m$^{-1}$ because $P$ during thunderstorms would be usually lower than 1 atm due to lower pressure system and hence gives $n < 1$. Since a uniform field, $\delta = H/\lambda$, gives $N_{\mathrm{RREA}} = S_0 \exp(H/\lambda)$, the factor $\eta = \exp(H/\lambda)$ is regarded as the avalanche multiplication factor, and becomes 3 and 30 for $H = 300$ and 1000 m, respectively. As a result, we obtain

$$N_{\mathrm{RREA}} = 2.2 \times 10^{11} \times (L/600\ \mathrm{m})^2 \times \Delta t/100\ \mathrm{s} \times \eta/30. \quad (6)$$

We thus obtain $N_{\mathrm{RREA}} = 10^{10}$–$10^{11}$, which agrees generally with the derived $N_e = 10^9$–$10^{11}$. Thus, the standard RREA process can explain at least the present two prolonged bursts.

[48] In the above estimation, we assumed that an electric field is slightly higher than the RREA threshold. However, a weaker field below this threshold might suffice to produce prolonged $\gamma$ ray emission. In reality, a 30–120 keV X-ray flux continuously increased, while an electric field is lower by 30%–60% than the RREA threshold [*Eack et al.*, 1996]. This quasi-static moderate-level field might be accomplished by, e.g., a charging mechanism of thunderclouds.

### 4.5. Comparisons With TGFs

[49] The derived $N_e$ (section 4.4) is more than 5 orders of magnitude lower than the number of relativistic electrons expected from TGF observations, e.g., $10^{16}$–$10^{17}$ [*Dwyer and Smith*, 2005]. This huge number of relativistic electrons in TGFs may be generated by relativistic feedback mechanism, involving positrons and X rays propagating in the opposite direction to runaway electrons [*Dwyer*, 2007, 2008]. Since the estimated $N_e$ of the present bursts is in general agreement with $N_{\mathrm{RREA}}$ expected from the simple RREA mechanism, we conclude that at least the present two events do not require an intense feedback process.

[50] In order to better characterize $\gamma$ ray spectra of long-duration events, we stacked count spectra over three bursts, namely, the present two ones and 070106 [*Tsuchiya et al.*, 2007]. Figure 13 compares the summed GROWTH spectrum with averaged TGF ones obtained by two independent satellites: one sums 289 events measured by Reuven Ramaty High Energy Solar Spectroscopic Imager (RHESSI) [*Dwyer and Smith*, 2005] and the other averages over 34 events observed by the Astrorivelatore Gamma a Immagini Leggero (AGILE) satellite [*Marisaldi et al.*, 2010a]. Thus, the composite GROWTH spectrum is rather similar in shape to those from TGFs, although three spectra all include detector responses. This resemblance is consistent with our basic standpoint [*Tsuchiya et al.*, 2007, 2009] that the long-duration $\gamma$ rays are emitted by the same bremsstrahlung process as TGFs.

[51] On a close comparison, the TGF spectra, especially the AGILE one, appear to have a higher cutoff energy than the GROWTH spectrum. This may be attributable to a difference in the electric potential operating in an acceleration region [*Dwyer and Smith*, 2005]. Thus, electrons accelerated in a much lower atmospheric density at the production sites of TGFs, 15–40 km [*Dwyer and Smith*, 2005; *Carlson et al.*, 2007; *Østgaard et al.*, 2008], would propagate through a longer distance, which gives a higher electric potential, and gain higher energies because of a smaller ionization loss per unit length.

## 5. Summary

[52] The GROWTH experiment observed two long-duration $\gamma$ ray emissions from winter thunderstorms on 13 December 2007 and 25 December 2008. The photon spectra obtained in both events clearly extends to 10 MeV and are consistent with a scenario that accelerated electrons produce, via bremsstrahlung, the observed $\gamma$ rays. Adopting a power law function as the initial photon spectrum at the source, we have constrained the source distance as 290–560 m for 071213 and 110–690 m for 081225, both at 90% confidence level. These constraints agree with visible light observations, which show that the bottom of winter thunderclouds is usually located 200–800 m above sea level [*Goto and Narita*, 1992]. We have shown a possibility that the observed $\gamma$ ray beams move with winter thunderclouds and spread over ~600 m.

[53] We estimated the number of relativistic electrons to cause the present prolonged $\gamma$ ray emissions as $10^9$–$10^{11}$. These are in general agreement with those expected from the standard RREA mechanism triggered by secondary cosmic rays. The cumulative GROWTH spectrum, summed over the present two ones and another GROWTH event [*Tsuchiya et al.*, 2007], was found to be similar in basic spectral features with the averaged TGF spectra [*Dwyer and Smith*, 2005; *Marisaldi et al.*, 2010a].

[54] **Acknowledgments.** We thank members of radiation safety group at Kashiwazaki-Kariwa power station, Tokyo Electric Power Company, for supporting our experiment. This work is supported in part by the Special Research Project for Basic Science at RIKEN, titled "Investigation of Spontaneously Evolving Systems," and the Special Postdoctoral

Research Project for Basic Science at RIKEN. The work is also supported in part by Grant-in-Aid for Scientific Research (S) 18104004 and Grant-in-Aid for Young Scientists (B) 19740167.

## References


Agostinelli, S., et al. (2003), Geant4—A simulation toolkit, *Nucl. Inst. Methods A*, *506*, 250, doi:10.1016/S0168-9002(03)01368-8.

Alexeenko, V. V., N. S. Khaerdinov, A. S. Lidvansky, and V. B. Petkov (2002), Transient variations of secondary cosmic rays due to atmospheric electric field and evidence for pre-lightning particle acceleration, *Phys. Lett. A*, *301*, 299, doi:10.1016/S0375-9601(02)00981-7.

Babich, L. P., E. N. Donskoi, I. M. Kutsyk, and R. A. Roussel-Dupré (2005), The feedback mechanism of runaway air breakdown, *Geophys. Res. Lett.*, *32*, L09809, doi:10.1029/2004GL021744.

Babich, L. P., E. N. Donskoy, and R. A. Roussel-Dupré (2007), Study of relativistic electron avalanche enhancement in the atmosphere at low overvoltages due to avalanche bremsstrahlung, *Geomagn. Aeron.*, *47*, 515, doi:10.1134/S0016793207040135.

Babich, L. P., E. I. Bochkov, E. N. Donskoi, and I. M. Kutsyk (2010), Source of prolonged bursts of high-energy gamma rays detected in thunderstorm atmosphere in Japan at the coastal area of the Sea of Japan and on high mountaintop, *J. Geophys. Res.*, *115*, A09317, doi:10.1029/2009JA015017.

Bell, T. F., V. P. Pasko, and U. S. Inan (1995), Runaway electrons as a source of Red sprites in the mesosphere, *Geophys. Res. Lett.*, *22*, 2127, doi:10.1029/95GL02239.

Briggs, M. S., et al. (2010), First results on terrestrial gamma ray flashes from the Fermi Gamma-ray Burst Monitor, *J. Geophys. Res.*, *115*, A07323, doi:10.1029/2009JA015242.

Brunetti, M., S. Cecchini, M. Galli, G. Giovannini, and A. Pagliarin (2000), Gamma-ray bursts of atmospheric origin in the MeV energy range, *Geophys. Res. Lett.*, *27*, 1599, doi:10.1029/2000GL003750.

Carlson, B. E., N. G. Lehtinen, and U. S. Inan (2007), Constraints on terrestrial gamma ray flash production from satellite observation, *Geophys. Res. Lett.*, *34*, L08809, doi:10.1029/2006GL029229.

Chilingarian, A., A. Daryan, K. Arakelyan, A. Hovhannisyan, B. Mailyan, L. Melkumyan, G. Hovsepyan, S. Chilingaryan, A. Reymers, and L. Vanyan (2010), Ground-based observations of thunderstorm-correlated fluxes of high-energy electrons, gamma rays, and neutrons, *Phys. Rev. D*, *82*, 043009, doi:10.1103/PhysRevD.82.043009.

Chubenko, A. P., et al. (2000), Intensive X-ray emission bursts during thunderstorms, *Phys. Lett. A*, *275*, 90, doi:10.1016/S0375-9601(00)00502-8.

Chubenko, A. P., et al. (2009), Energy spectrum of lightning gamma emission, *Phys. Lett. A*, *373*, 2953, doi:10.1016/j.physleta.2009.06.031.

Connaughton, V., et al. (2010), Associations between Fermi Gamma-ray Burst Monitor terrestrial gamma ray flashes and sferics from the World Wide Lightning Location Network, *J. Geophys. Res.*, *115*, A12307, doi:10.1029/2010JA015681.

Dwyer, J. R. (2003), A fundamental limit on electric fields in air, *Geophys. Res. Lett.*, *30*(20), 2055, doi:10.1029/2003GL017781.

Dwyer, J. R. (2007), Relativistic breakdown in planetary atmosphere, *Phys. Plasmas*, *14*, 042901, doi:10.1063/1.2709652.

Dwyer, J. R. (2008), Source mechanisms of terrestrial gamma-ray flashes, *J. Geophys. Res.*, *113*, D10103, doi:10.1029/2007JD009248.

Dwyer, J. R., and D. M. Smith (2005), A comparison between Monte Carlo simulations of runaway breakdown and terrestrial gamma-ray flash observations, *Geophys. Res. Lett.*, *32*, L22804, doi:10.1029/2005GL023848.

Dwyer, J. R., et al. (2003), Energetic radiation produced during rocket-triggered lightning, *Science*, *299*, 694, doi:10.1126/science.1078940.

Dwyer, J. R., et al. (2004a), Measurements of x-ray emission from rocket-triggered lightning, *Geophys. Res. Lett.*, *31*, L05118, doi:10.1029/2003GL018770.

Dwyer, J. R., et al. (2004b), A ground level gamma-ray burst observed in association with rocket-triggered lightning, *Geophys. Res. Lett.*, *31*, L05119, doi:10.1029/2003GL018771.

Dwyer, J. R., et al. (2005), X-ray bursts associated with leader steps in cloud-to-ground lightning, *Geophys. Res. Lett.*, *32*, L01803, doi:10.1029/2004GL021782.

Eack, K. B., W. H. Beasley, R. W. David, T. C. Marshall, and M. Stolzenburg (1996), Initial results from simultaneous observation of X rays and electric fields in a thunderstorms, *J. Geophys. Res.*, *101*, 29,637, doi:10.1029/96JD01705.

Eack, K. B., D. M. Suszcynsky, W. H. Beasley, R. Roussel-Dupre, and E. Symbalisty (2000), Gamma-ray emissions observed in a thunderstorm anvil, *Geophys. Res. Lett.*, *27*, 185, doi:10.1029/1999GL010849.

Enoto, T., et al. (2007), Detection of gamma-rays from winter thunderclouds along the coast of Japan Sea, *Proc. Int. Cosmic Ray. Conf.*, *30*, 745.

Fishman, G. J., et al. (1994), Discovery of intense gamma-ray flashes of atmospheric origin, *Science*, *264*, 1313, doi:10.1126/science.264.5163.1313.

Goto, Y., and K. Narita (1992), Observations of winter lightning to an isolate tower, *Res. Lett. Atmos. Electr.*, *12*, 57.

Grefenstette, B. W., D. M. Smith, B. J. Hazelton, and L. I. Lopez (2009), First RHESSI terrestrial gamma ray flash catalog, *J. Geophys. Res.*, *114*, A02314, doi:10.1029/2008JA013721.

Grieder, P. K. F. (2001), *Cosmic Rays at Earth*, p. 198, Elsevier Sci., Amsterdam.

Gurevich, A. V., G. M. Milikh, and R. A. Roussel-Dupré (1992), Runaway electron mechanism of air breakdown and preconditioning during a thunderstorm, *Phys. Lett. A*, *165*, 463, doi:10.1016/0375-9601(92)90348-P.

Gurevich, A. V., G. M. Milikh, and J. A. Valdivia (1997), Model of X-ray emission and fast preconditioning during a thunderstorm, *Phys. Lett. A*, *231*, 402, doi:10.1016/S0375-9601(97)00354-X.

Gurevich, A. V., K. P. Zybin, and Y. V. Medvedev (2007), Runaway breakdown in strong electric field as a source of terrestrial gamma flashes and gamma bursts in lightning leader steps, *Phys. Lett. A*, *361*, 119, doi:10.1016/j.physleta.2006.05.063.

Heck, D., and T. Pierog (2009), *Extensive Air Shower Simulation with CORSIKA: A User's Guide*, 114 pp., Forschungszent. Karlsruhe, Karlsruhe, Germany.

Heck, D., et al. (1998), Report FZKA 6019, Forschungszent. Karlsruhe, Karlsruhe, Germany.

Howard, J., M. A. Uman, J. R. Dwyer, D. Hill, C. Biagi, Z. Saleh, J. Jerauld, and H. K. Rassoul (2008), Co-location of lightning leader x-ray and electric field change sources, *Geophys. Res. Lett.*, *35*, L13817, doi:10.1029/2008GL034134.

Kitagawa, N., and K. Michimoto (1994), Meteorological and electrial aspects of winter thunderclouds, *J. Geophys. Res.*, *99*, 10,713, doi:10.1029/94JD00288.

Koch, H. W., and J. W. Motz (1959), Bremsstrahlung cross-section formulas and related data, *Rev. Mod. Phys.*, *31*, 920, doi:10.1103/RevModPhys.31.920.

Lehtinen, N. G., M. Walt, U. S. Inan, T. F. Bell, and V. P. Pasko (1996), $\gamma$-ray emission produced by a relativistic beam of runaway electrons accelerated by quasi-electrostatic thundercloud fields, *Geophys. Res. Lett.*, *23*, 2645, doi:10.1029/96GL02573.

Lehtinen, N. G., T. F. Bell, and U. S. Inan (1999), Monte Carlo simulation of runaway MeV electron breakdown with application to red sprites and terrestrial gamma ray flashes, *J. Geophys. Res.*, *104*, 24,699, doi:10.1029/1999JA900335.

Marisaldi, M., et al. (2010a), Detection of terrestrial gamma ray flashes up to 40 MeV by the AGILE satellite, *J. Geophys. Res.*, *115*, A00E13, doi:10.1029/2009JA014502.

Marisaldi, M., et al. (2010b), Gamma-ray localization of terrestrial gamma-ray flashes, *Phys. Rev. Lett.*, *105*, 128501, doi:10.1103/PhysRevLett.105.128501.

McCarthy, M. P., and G. K. Parks (1985), Further observations of X-rays inside thunderstorms, *Geophys. Res. Lett.*, *12*, 393, doi:10.1029/GL012i006p00393.

Milikh, G., and J. A. Valdivia (1999), Model of gamma ray flashes due to fractal lightning, *Geophys. Res. Lett.*, *26*, 525, doi:10.1029/1999GL900001.

Moore, C. B., K. B. Eack, G. D. Aulich, and W. Rison (2001), Energetic radiation associated with lightning stepped-leaders, *Geophys. Res. Lett.*, *28*, 2141, doi:10.1029/2001GL013140.

Muraki, Y., et al. (2004), Effects of atmospheric electric fields on cosmic rays, *Phys. Rev. D*, *69*, 123010, doi:10.1103/PhysRevD.69.123010.

Nelson, W. R., H. Hirayama, and D. W. O Rogers (1985), The EG84 code system, *Rep. SLAC-265*, Stanford Univ., Stanford, Calif.

Østgaard, N., T. Gjesteland, J. Stadsnes, P. H. Connell, and B. Carlson (2008), Production altitude and time delays of the terrestrial gamma flashes: Revisiting the Burst and Transient Source Experiment spectra, *J. Geophys. Res.*, *113*, A02307, doi:10.1029/2007JA012618.

Rakov, V. A., and M. A. Uman (2005), Winter lightning in Japan, in *Lightning Physics and Effects*, 3rd ed., p. 308, Cambridge Univ. Press, Cambridge, U. K.

Roussel-Dupré, R. A., and A. V. Gurevich (1996), On runaway breakdown and upward propagating discharges, *J. Geophys. Res.*, *101*, 2297, doi:10.1029/95JA03278.

Roussel-Dupré, R. A., A. V. Gurevich, T. Tunnell, and G. M. Milikh (1994), Kinetic theory of runaway air breakdown, *Phys. Rev. E*, *49*, 2257, doi:10.1103/PhysRevE.49.2257.

Roussel-Dupré, R., J. J. Colman, E. Symbalisty, D. Sentman, and V. P. Pasko (2008), Physical processes related to discharges in planetary atmosheres, *Space Sci. Rev.*, *137*, 51, doi:10.1007/s11214-008-9385-5.

Smith, D. M., L. I. Lopez, R. P. Lin, and C. P. Barrington-Leigh (2005), Terrestrial gamma-ray flashes observed up to 20 MeV, *Science*, *307*, 1085, doi:10.1126/science.1107466.

Suszcynsky, D. M., R. Roussel-Dupré, and C. Shaw (1996), Ground-based search for X rays generated by thunderstorms and lightning, *J. Geophys. Res.*, *101*, 23,505, doi:10.1029/96JD02134.

Torii, T., M. Takeishi, and T. Hosono (2002), Observation of gamma-ray dose increase associated with winter thunderstorm and lightning activity, *J. Geophys. Res.*, *107*(D17), 4324, doi:10.1029/2001JD000938.

Torii, T., T. Sugita, S. Tanabe, Y. Kimura, M. Kamogawa, K. Yajima, and H. Yasuda (2009), Gradual increase of energetic radiation associated with thunderstorm activity at the top of Mt. Fuji, *Geophys. Res. Lett.*, *36*, L13804, doi:10.1029/2008GL037105.

Tsuchiya, H., et al. (2007), Detection of high-energy gamma rays from winter thunderclouds, *Phys. Rev. Lett.*, *99*, 165002, doi:10.1103/PhysRevLett.99.165002.

Tsuchiya, H., et al. (2009), Observation of an energetic radiation burst from mountain-top thunderclouds, *Phys. Rev. Lett.*, *102*, 255003, doi:10.1103/PhysRevLett.102.255003.

Yamazaki, K., S. Tonouchi, and T. Hashimoto (2002), Factors associated with the variations in environmental gamma-ray spectra in Kashiwazaki Kariwa area, *J. Radioanal. Nucl. Chem.*, *252*, 359, doi:10.1023/A:1015734810119.

Yoshida, S., T. Morimoto, T. Ushio, Z.-I. Kawasaki, T. Torii, D. Wang, N. Takagi, and T. Watanabe (2008), High energy photon and electron bursts associated with upward lightning strokes, *Geophys. Res. Lett.*, *35*, L10804, doi:10.1029/2007GL032438.

Yoshioka, K. (1992), The seasonal variation of rainout activity of short-lived radon daughters, *Radiat. Prot. Dosim.*, *45*, 395.

T. Enoto, Kavli Institute for Particle Astrophysics and Cosmology, Department of Physics and SLAC National Accelerator Laboratory, Stanford University, Stanford, CA 94305, USA. (enoto@stanford.edu)

H. Kato, M. Okano, and H. Tsuchiya, High-energy Astrophysics Laboratory, RIKEN, 2-1, Hirosawa, Wako, Saitama 351-0198, Japan. (hkato@riken.jp; mokano@crab.riken.jp; htsuchiya@riken.jp)

M. Kawaharada and M. Kokubun, Department of High Energy Astrophysics, Institute of Space and Astronautical Science, JAXA, 3-1-1, Chuo-ku, Sagamihara, Kanagawa 252-5210, Japan. (kawahard@astro.isas.jaxa.jp; kokubun@astro.isas.jaxa.jp)

T. Kitaguchi, Division of Physics, Mathematics, and Astronomy, California Institute of Technology, 1200 East California Blvd., Pasadena, CA 91125, USA. (kitaguti@caltech.edu)

K. Makishima, K. Nakazawa, S. Yamada, and T. Yuasa, Department of Physics, University of Tokyo, 7-3-1, Hongo, Bunkyo-ku, Tokyo 113-0033, Japan. (maxima@phys.s.u-tokyo.ac.jp; nakazawa@phys.s.u-tokyo.ac.jp; yamada@juno.phys.s.u-tokyo.ac.jp; yuasa@juno.phys.s.u-tokyo.ac.jp)